Title

The hepatic compensatory response to elevated systemic sulfide impairs medium chain fat oxidation and promotes diabetes.

Authors

Roderick N. Carter[1], Matthew T.G. Gibbins[1,a], Martin E. Barrios-Llerena[1,b], Stephen E. Wilkie[1,2], Peter L. Freddolino[3], Marouane Libiad[3,c], Victor Vitvitsky[3], Barry Emerson[1,d], Thierry Le Bihan[4,e], Madara Brice[1], Huizhong Su[5,f], Scott Denham[1], Natalie Z.M. Homer[1], Clare Mc Fadden[1,g], Anne Tailleux[6], Nourdine Faresse[7,h], Thierry Sulpice[7], Francois Briand[7], Tom Gillingwater[8], Kyo Han Ahn[9], Subhankar Singha[9,i], Claire McMaster[10], Richard C. Hartley[10], Bart Staels[6], Gillian Gray[1], Andrew J. Finch[5,j], Colin Selman[2], Ruma Banerjee[3], Nicholas M. Morton[1*]

[1]University/British Heart Foundation Centre for Cardiovascular Science, University of Edinburgh, Queen's Medical Research Institute, Edinburgh, EH16 4TJ, United Kingdom
[2]Glasgow Ageing Research Network (GARNER), Institute of Biodiversity, Animal Health and Comparative Medicine, University of Glasgow, Glasgow, G12 8QQ, United Kingdom
[3]The Department of Biological Chemistry, University of Michigan Medical School, Ann Arbor, MI 48109, USA
[4]SynthSys - Systems and Synthethic Biology, Edinburgh, EH9 3JD, United Kingdom
[5]Cancer Research UK Edinburgh Centre, MRC Intitute of Genetics & Molecular Medicine, University of Edinburgh, Western General Hospital, Edinburgh, EH4 2XR, United Kingdom
[6]Université de Lille, Inserm, CHU Lille, Institut Pasteur de Lille, U101-EGID, F-59000, Lille, France
[7]Physiogenex S.A.S, Prologue Biotech, 516 rue Pierre et Marie Curie, 31670 Labège, France
[8]College of Medicine & Veterinary Medicine, University of Edinburgh, Old Medical School (Anatomy), Teviot Place, Edinburgh, EH8 9AG, United Kingdom
[9]Department of Chemistry, POSTECH, 77 Cheongam-Ro, Nam-Gu, Pohang, Gyungbuk, 37673, South Korea
[10]School of Chemistry, Joseph Black Building, University of Glasgow, Glasgow, G12 8QQ, United Kingdom

Current affiliations where different from the place where work for the manuscript was carried out;
[a]Cambridge Biomedical Campus, Royal Papworth Hospital NHS Foundation Trust, Cardiology department, Cambridge, CB2 0AY, United Kingdom
[b]The International Clinical Research Centre, St. Anne's University Hospital, Brno, 656 91, Czech Republic
[c]Institute for Integrative Biology of the Cell (I2BC), CEA, CNRS, Univ. Paris-Sud, Université Paris-Saclay, 91198, Gif-sur-Yvette cedex, France
[d]BD Research Centre Ireland, Co. Limerick, Castletroy, Ireland
[e]Rapid Novor Inc, 44 Gaukel St, Kitchener, ON N2G 4P3, Canada
[f]Wellcome Trust Centre for Mitochondrial Research, Newcastle University, NE2 4HH, United Kingdom
[g]Springer Nature Campus, London, N1 9FN, United Kingdom
[h]D.I.V.A-expertise, 1 place Pierre Potier, 31100 Toulouse, France
[i]Institute of Advanced Studies and Research, JIS University, Kolkata 700091, India
[j]Cancer Research UK Barts Centre, London, EC1M 6BQ, United Kingdom

[*]**Lead Contact details**: Nicholas M Morton
Molecular Metabolism Group, University/British Heart Foundation Centre for Cardiovascular Science, University of Edinburgh, Queen's Medical Research Institute, Edinburgh, EH16 4TJ, United Kingdom.
nik.morton@ed.ac.uk

Competing interests statement,

The authors have declared that no conflict of interest exists.

Abstract

Impaired hepatic glucose and lipid metabolism are hallmarks of type–2 diabetes. Increased sulfide production from cysteine, or sulfide–donor compounds, may beneficially regulate hepatic metabolism. Disposal of sulfide through the sulfide oxidation pathway (SOP) is critical for maintaining sulfide within a safe physiological range. We show that mice lacking the liver–enriched mitochondrial SOP enzyme thiosulfate sulfur–transferase (*Tst*$^{-/-}$ mice) exhibit high circulating sulfide, increased gluconeogenesis, hypertriglyceridemia and fatty liver, despite whole–body insulin–sensitisation. Unexpectedly, hepatic sulfide levels were normal in *Tst*$^{-/-}$ mice, a result of homeostatic induction of mitochondrial sulfide disposal and glutathione excretion associated with net suppression of protein persulfidation and nuclear respiratory factor–2 target proteins. Proteomic and persulfidomic profiling converged on hepatic lipid metabolism, revealing a deficit in medium–chain fatty acid oxidation in *Tst*$^{-/-}$ mice. In conclusion our findings have implications for sulfide-donor strategies in the context of liver function and metabolic disease.

65 # Introduction

66 The prevalence of Type 2 diabetes (T2D) continues to soar in parallel with that of obesity[1].
67 Increased hepatic glucose production and aberrant hepatic lipid metabolism are cardinal
68 features of T2D[2,3]. Dysregulation of hepatic nutrient metabolism in T2D is a promising area
69 for therapeutic intervention because it precipitates the more severe liver pathologies that
70 manifest along the spectrum of non-alcoholic fatty liver disease (NAFLD), steatosis,
71 steatohepatitis and hepatocellular carcinoma[4].

72 Hydrogen sulfide (hereafter referred to as sulfide), an endogenously produced gaseous
73 signalling molecule[5–8], has recently emerged as a modulator of nutrient metabolism[9–12].
74 Enzymatic sulfide production from sulfur amino acids is catalysed by cystathionine beta–
75 synthase; CBS, and cystathionine gamma lyase; CTH[13,14] and by 3-mercaptopyruvate sulfur
76 transferase; MPST[15–17]. Thioredoxin-mediated reduction of cysteine persulfides on proteins
77 also regulates free sulfide and cysteine persulfide levels[18]. Endogenously produced and
78 exogenously administered sulfide specifically influences hepatic glucose and lipid
79 metabolism[19,20]. Thus, *in vitro,* treatment of murine hepatocytes with NaHS, or
80 overexpression of rat *Cth* in HepG2 liver cells, increased glucose production through increased
81 gluconeogenesis and reduced glycogen storage[21]. Conversely, glucose production was lower
82 in hepatocytes from *Cth* gene knockout mice ($Cth^{-/-}$ mice) that exhibit low sulfide
83 production[21]. Elevation of sulfide with NaHS administration *in vivo* reduced cholesterol and
84 triglyceride accumulation in the liver of high fat diet (HFD)–fed mice[22]. In contrast, inter-cross
85 of sulfide production–deficient $Cth^{-/-}$ mice with the hyperlipidemic $Apoe^{-/-}$ mouse strain
86 ($Cth^{-/-}Apoe^{-/-}$ mice) produced a phenotype of elevated plasma cholesterol following
87 exposure to an atherogenic diet[23]. Consistent with their higher cholesterol, $Cth^{-/-}Apoe^{-/-}$
88 mice developed fatty streak lesions earlier than $Apoe^{-/-}$ mice, and this effect was reversed

89 by NaHS administration[23]. Sulfide may also indirectly impact hepatic nutrient metabolism
90 through its effect on hepatic artery vasorelaxation and thus liver perfusion[24,25]. The
91 apparently beneficial effects of sulfide administration in multiple disease indications has led
92 to a major drive towards development of targeted H_2S–donor molecules as a therapeutic
93 approach[26,27]. However, an often-overlooked aspect of net sulfide exposure, key to the
94 efficacy of therapeutic H_2S–donors, is that it is regulated through its oxidative disposal. Thus,
95 endogenous sulfide exposure is actively limited to prevent mitochondrial respiratory
96 toxicity[28–30]. Sulfide is rapidly oxidized[31,32] through the mitochondrial sulfide oxidation
97 pathway (SOP), consisting of sulfide quinone oxidoreductase (SQOR), persulfide dioxygenase
98 (ETHE1/PDO) and thiosulfate sulfurtransferase (TST, also known as rhodanese)[31,33,34]. The
99 liver is highly abundant in SOP enzymes, and is a major organ of whole body sulfide disposal[32].
100 Mice lacking the *Ethe1* gene (*Ethe1*$^{-/-}$ mice) die of fatal sulfide toxicity[30], consistent with its
101 critical role in sulfide oxidation and the severe pathological consequences of unchecked
102 sulfide build-up in tissues. However, the importance of mitochondrial TST in the SOP *in vivo*
103 remains obscure. In contrast to *Ethe1*$^{-/-}$ mice, *Tst*$^{-/-}$ mice were grossly normal despite
104 exhibiting substantially elevated blood sulfide levels, as implied by qualitative measures[35].
105 This revealed an important yet distinct role for TST in the SOP for the first time *in vivo*.
106 Nevertheless, *Tst*$^{-/-}$ mice showed an apparently diabetogenic impairment of glucose
107 tolerance[35], consistent with the concept that increased sulfide promotes hepatic glucose
108 production[21]. As *Tst* deficiency represents a model of chronic but viable sulfide elevation,
109 determining the molecular mechanisms driving their aberrant metabolic profile can provide
110 important insights into the optimal range for therapeutic sulfide exposure, particularly in light
111 of the current interest in developing mitochondrially–targeted sulfide–donors[36,37]. To this end

112 we sought to define the impact of *Tst* deficiency on the underlying molecular pathways that

113 impact hepatic metabolism.

114

115 # Results

116 *Tst*$^{-/-}$ *mice exhibit increased hepatic gluconeogenesis and dyslipidaemia despite peripheral*
117 *insulin sensitisation.* TST *mRNA* expression is highest in the liver (e.g. it is ~8-fold higher than
118 in white adipose tissue http://biogps.org/#goto=genereport&id=22117). We therefore
119 hypothesised that liver TST deficiency was the principal driver of the impaired glucose
120 tolerance observed in *Tst*$^{-/-}$ mice[35]. We first tested this by challenging the mice with
121 pyruvate, which is converted to glucose in the liver. *Tst*$^{-/-}$ mice exhibited higher glucose
122 production than C57BL/6J controls in response to pyruvate (Figure 1A). We next tested
123 phosphoenolpyruvate carboxykinase (PEPCK) activity, the rate-determining enzyme in *de-*
124 *novo* hepatic glucose synthesis, and found it was higher in liver homogenates from *Tst*$^{-/-}$
125 mice (Figure 1B). Next, we traced the metabolite incorporation of $^{13}C_3$-pyruvate by isolated
126 *Tst*$^{-/-}$ hepatocytes, which showed a significant reduction in $^{13}C_2$-acetyl-CoA and a significant
127 increase in $^{13}C_3$-aspartate, consistent with skewing of the tricarboxylic acid cycle towards
128 gluconeogenic precursors (Figure 1C). We also assessed whether *Tst* deficiency is associated
129 with impaired lipid metabolism, another hallmark of diabetes. Fast protein liquid
130 chromatography analysis of triglyceride levels and their lipoprotein distribution revealed
131 significantly higher total plasma triglycerides in *Tst*$^{-/-}$ mice (Figure 1D). The higher
132 triglyceride was selectively associated with an increased VLDL triglyceride fraction (Figure 1D),
133 consistent with a dominant liver-driven impairment in lipid metabolism[38]. Total and distinct
134 lipoprotein fraction plasma cholesterol levels were similar between genotypes (Figure S1A
135 and S1B), suggestive of a triglyceride–selective effect of *Tst* deficiency on hepatic lipid efflux.
136 HFD significantly increased liver lipid content of C57BL/6J mice but did not further increase
137 the lipid levels in the liver of *Tst*$^{-/-}$ mice (Figure 1E-1F). Liver glycogen, a marker of long–term

138 carbohydrate storage was comparable between *Tst*$^{-/-}$ and C57BL/6J control mice (Figure
139 S1C). Steady–state phosphorylation levels of hepatic insulin–responsive proteins AKT and the
140 cellular energy–sensing protein AMPK were comparable between *Tst*$^{-/-}$ mice and C57BL/6J
141 littermates (Figure S1D).

142 Despite unchanged steady–state markers of hepatic insulin sensitivity, impaired glucose
143 tolerance suggested that whole body, and usually hepatic, insulin–resistance was present. To
144 test this, we performed an insulin tolerance test. Unexpectedly, the glucose decrement in
145 response to insulin was greater in *Tst*$^{-/-}$ mice (Figure 1G), demonstrating a net increase in
146 dynamic whole–body insulin sensitivity despite increased hepatic glucose output. We
147 confirmed increased whole–body insulin sensitivity under short–term steady–state
148 conditions using euglycaemic hyperinsulinaemic clamps. Blood glucose tended to be higher
149 in the *Tst*$^{-/-}$ mice during baseline conditions (Figure 1H). During the clamp, when blood
150 glucose levels were maintained constant, the glucose infusion rate was comparable between
151 genotypes (Table S1). However, an overall increase in glucose uptake (integral glucose) by
152 tissues in the *Tst*$^{-/-}$ mice was apparent (Figure 1I, Table S1), supporting increased peripheral
153 insulin–sensitivity concurrent with higher endogenous glucose production. After HFD feeding,
154 *Tst*$^{-/-}$ mice exhibited relatively lower fasting insulin and higher hepatic glucose output across
155 baseline pre-clamp conditions (Table S2). However, the metabolic phenotype of *Tst*$^{-/-}$ mice
156 largely converged on that of the C57BL/6J mice during the hyperinsulinemic clamp (Table S2).

157 *TST deficiency elicits compensatory hepatic sulfide disposal mechanisms that drive reduced*
158 *global protein persulfidation.* A role for TST in the disposal of sulfide was suggested by its
159 participation in the SOP[31,34] and supported *in vivo* by the qualitatively higher blood sulfide of
160 *Tst*$^{-/-}$ mice[35]. Here, we quantified circulating sulfide, showing approximately 10–fold
161 elevation in the blood and plasma of *Tst*$^{-/-}$ mice (Table 1A and 1B). Thiosulfate, an oxidised

162 metabolite of sulfide [39,40] and a TST substrate[41], was approximately 20–fold higher in plasma
163 (Table 1B), and profoundly higher (450–fold) in urine (Table 1C) of *Tst*$^{-/-}$ mice compared to
164 C57Bl/6J mice. Reduced glutathione (GSH) levels were ~2–fold higher in the plasma of *Tst*$^{-/-}$
165 mice (Table 1B). To determine any direct hepatic contribution to the elevated systemic sulfide
166 *in vivo*, whole blood was sampled from the inferior vena cava (IVC) (Table 1D). IVC sulfide
167 levels tended to be higher in the *Tst*$^{-/-}$ mice, but the magnitude of the increase (~3-fold) did
168 not parallel that in trunk blood (~10-fold), suggesting liver was not a major source of the
169 elevated circulating sulfide. Surprisingly, liver sulfide, thiosulfate, cysteine and GSH levels
170 were similar between *Tst*$^{-/-}$ and C57BL/6J mice (Table 1E). Further, cultured hepatocytes
171 from *Tst*$^{-/-}$ and C57BL/6J mice exhibited similar intracellular sulfide levels, as estimated
172 using P3, a sulfide–selective fluorescent probe[42] (Table 1F). Mitochondrial sulfide levels in
173 liver reported by MitoA/MitoN[43] were similarly unchanged between genotypes (Table 1G).
174 The apparently unaltered hepatic steady-state sulfide levels, despite higher circulating
175 sulfide, suggested a profound homeostatic mechanism was invoked in the liver of *Tst*$^{-/-}$
176 mice. We assessed respiratory sulfide disposal (antimycin–sensitive) and found this was
177 markedly increased in hepatocytes from *Tst*$^{-/-}$ mice, whereas antimycin–insensitive sulfide
178 disposal was relatively reduced compared to hepatocytes from C57BL/6J mice (Table S3).
179 Isolated liver mitochondria from *Tst*$^{-/-}$ hepatocytes also exhibited a higher sulfide disposal
180 rate (Table S3). In addition, cysteine and GSH was excreted at higher levels from *Tst*$^{-/-}$
181 hepatocytes under basal conditions and after stimulation of sulfur amino acid metabolism by
182 addition of methionine (Figure 2A and 2B). Consistent with higher GSH turnover, hepatocytes
183 from *Tst*$^{-/-}$ mice showed resistance to exogenous H_2O_2–mediated mitochondrial ROS
184 production (Figure S2). We next determined the global hepatic protein persulfidation profile,
185 the major post–translational modification mediated by sulfide[44–46]. Mass spectrometry

186 analysis of maleimide–labelled liver peptides revealed a greater abundance of peptides with
187 a lower persulfidation level (under-persulfidated) in the liver of *Tst*$^{-/-}$ mice (Figure 2C). We
188 confirmed this using semi-quantitative western–blot analysis on pulled down maleimide–
189 labelled proteins (Figure 2D). Gene Ontology (GO) analysis of proteins exhibiting altered
190 persulfidation levels revealed 28 terms different between *Tst*$^{-/-}$ and C57BL/6J mice by log–
191 fold change (Table 2). Major under-persulfidated terms (20) included "*FAD-binding*, *methyl*
192 *transferase, peroxisome, acyl-CoA dehydrogenase activity and transaminase*" while the less
193 abundant (8) over-persulfidated terms were dominated by terms related to "*Nicotinamide*
194 *metabolism*".

195 *The hepatic proteome of Tst*$^{-/-}$ *mice reveals a distinct molecular signature of altered sulfur*
196 *and mitochondrial nutrient metabolism.* To gain molecular insight into the mechanisms
197 underlying the apparently diabetogenic liver phenotype in ND-fed *Tst*$^{-/-}$ mice, we performed
198 a comparative iTRAQ proteomic analysis of whole liver with ND-fed C57BL/6J mice. Kyoto
199 Encyclopedia of Genes and Genomes (KEGG) analysis (at significance threshold $P < 0.05$)
200 revealed 4 up–regulated pathways in liver of *Tst*$^{-/-}$ mice related to amino acid metabolism,
201 including sulfur amino acids, and sulfur metabolism (Table 3A). GO analysis (at threshold $P <$
202 0.05) revealed 95 significantly up–regulated terms in liver of *Tst*$^{-/-}$ mice (Table S4A). Of the
203 top 14 up–regulated terms, 7 referred to amino acid metabolism and 1 referred to the
204 organellar term '*mitochondrion*'. KEGG pathway analysis revealed 27 down–regulated
205 pathways in the liver of *Tst*$^{-/-}$ mice (Table 3B) including Phase 1 and 2 detoxification
206 pathways (Cytochrome P450s, Glutathione and Glucuronidation) and '*Lysosome*', '*Protein*
207 *processing in the Endoplasmic reticulum'* organellar terms. 213 GO terms were significantly
208 down–regulated in *Tst*$^{-/-}$ mice (Table S4B). Among the most significant down–regulated
209 terms were phase 2 detoxification pathways such as *'glutathione binding'* and '*glutathione*

210 *transferase activity'* and '*endoplasmic reticulum'*. We validated a representative subset of
211 protein changes (Figures S3A), noting broadly consistent direction of change in the key
212 pathways. At the single protein level, the most robust change we observed was increased
213 MPST protein in whole liver (Figure S3A) and mitochondrial sub-fractions (Figure S3B). This
214 change was remarkable as mRNA levels for *Mpst* were lower in *Tst*$^{-/-}$ mice (Figure S3C), likely
215 as a result of loss of proximal *Mpst* promoter function; *Mpst* is a paralog of *Tst*[47] juxtaposed
216 approximately 1kb from *Tst*. Given the evidence for glucose and lipid metabolic changes in
217 the *Tst*$^{-/-}$ mice, we undertook a further focussed comparison of canonical proteins in these
218 pathways (Table S5). Four GO terms were enriched in liver from *Tst*$^{-/-}$ mice, all of which were
219 down–regulated; '*Lipid metabolic process'*, *'fatty acid beta-oxidation'*, *'Acyl-CoA*
220 *dehydrogenase activity' and 'Acyl-CoA hydrolase activity'* (Table S5).

221 *Hepatic protein expression in Tst*$^{-/-}$ *mice is consistent with lower NRF2 activation***.** We
222 performed a transcription factor binding site (TFBS) enrichment analysis in the promoters of
223 proteins that are up–regulated in the liver of *Tst*$^{-/-}$ mice to look for potential hub
224 transcriptional drivers of the proteome profile (Figure S4A). This revealed a statistically
225 significant under-representation of TFBS for the sulfide–responsive[48,49] NRF2 transcription
226 factor (Figure S4A). To explore whether there was evidence for reduced NRF2 activation in
227 the *Tst*$^{-/-}$ liver, we looked at the relative expression of 47 NRF2–regulated proteins in the
228 proteome of ND-fed *Tst*$^{-/-}$ and ND-fed C57Bl/6J mice. While 37 of these target proteins were
229 similar in expression between the genotypes, 10 NRF2 target proteins were lower in *Tst*$^{-/-}$
230 liver (Figure S4B) and none of the 47 NRF2 target proteins were increased in *Tst*$^{-/-}$ liver.

231 *Proteome of TST deficiency versus HFD response in C57BL/6J mice reveals distinct regulation*
232 *of lipid metabolism and detoxification pathways.* We examined mechanistic commonalities

233 between the diabetogenic hepatic phenotype of *Tst*$^{-/-}$ mice and that induced by the
234 diabetogenic HFD–feeding regimen in C57BL/6J mice. Note, ND-fed *Tst*$^{-/-}$ mice were in a pre-
235 existing diabetogenic state (Figure 1) that does not further worsen with HFD (Figure 1E-F,
236 Table S1B), suggesting gross phenotypic convergence of the two genotypes after HFD. We
237 compared the identity and direction of change of the 188 proteins differentially expressed in
238 ND-fed *Tst*$^{-/-}$ mice (versus ND-fed C57BL/6J mice; Figure 3A) to proteins that were
239 differentially expressed in response to HFD in C57BL/6J mice (432 proteins; Figure 3A). There
240 was a striking 67% overlap in individual proteins (126) in this comparison (Figure 3A). When
241 we analysed these two protein signatures for directionally shared pathways, one KEGG
242 pathway *'Glycine, serine and threonine metabolism'* was up–regulated (Table S6A) and 12
243 KEGG pathways were down–regulated, including *'drug metabolism'* and *'endoplasmic*
244 *reticulum'* (Table S6B). Consistent with a pre-existing HFD–like proteome, the proteomic
245 response in the liver of *Tst*$^{-/-}$ mice to HFD was muted, relative to that observed in C57BL6J
246 mice (106 proteins, a 4–fold lower response; Figure 3B). We then considered contrasting,
247 rather than congruent, proteomic responses arising from TST deficiency versus HFD responses
248 in C57BL/6J mice to illuminate potential novel pathways underlying the otherwise functionally
249 similar overall diabetogenic hepatic *Tst*$^{-/-}$ phenotype. 5 KEGG pathways (Table S7A) and 4
250 GO terms (Table S7B) were regulated in the opposite direction in this comparison. Strikingly,
251 the GO terms were all related to lipid metabolism, which were up–regulated in the HFD
252 response, but down–regulated with TST deficiency (Table S7A-B). An organelle–focussed
253 protein analysis showed shared up-regulation of mitochondrial and endoplasmic reticulum
254 pathways between TST deficiency (Figure 3C upper row) and C57BL/6J HFD-responses (Figure
255 3C lower row), but a striking discordance in peroxisomal protein pathways (up-regulated by

256 HFD, down-regulated TST deficiency) and nuclear proteins (down-regulated by HFD, up-
257 regulated TST deficiency; Figure 3C).

258 *The Tst$^{-/-}$ liver proteome and persulfidome converge on transamination and lipid oxidation*
259 *pathways.* To assess whether conservation of changes at protein and post-translational
260 modification levels can illuminate key regulatory hubs driving the hepatic phenotype we ran
261 a congruence analysis of the proteome and persulfidome. We found that GO terms referring
262 to amino acid, lipid metabolism and peroxisome were significantly regulated at both the level
263 of protein abundance and persulfidation status (Table 4).

264 *Tst$^{-/-}$ hepatocytes exhibit elevated mitochondrial respiration and a defect in medium–chain*
265 *fatty acid oxidation.* Enhanced respiratory sulfide disposal was found from *Tst$^{-/-}$*
266 hepatocytes, and enrichment of mitochondrial proteins was suggested from the liver
267 proteome of the *Tst$^{-/-}$* mice (Table S4). We therefore sought to determine if TST deficiency
268 affected respiratory function and substrate utilisation of the hepatocyte. Analysis of electron
269 micrographs prepared from the liver of ND-fed *Tst$^{-/-}$* mice and C57BL/6J controls showed
270 morphologically normal mitochondria (Figure 4A). Basal respiration, comprising ATP–linked
271 and leak respiration, was significantly higher in hepatocytes from *Tst$^{-/-}$* mice (Figure 4B–4D).
272 Maximal hepatocyte respiratory capacity and non–respiratory oxygen consumption was
273 similar between genotypes (Figures S5A and S5B). In line with phenotypic convergence
274 following HFD, hepatocyte respiration was comparable between genotypes from HFD-fed
275 mice (Figures S5C-S5H). A unique feature of the liver from *Tst$^{-/-}$* mice that contrasted with
276 HFD response in C57BL/6J mice was a decrease in proteins and persulfidation levels of
277 proteins in lipid oxidation pathways. We therefore investigated hepatocyte respiration of
278 lipids. Using a low pyruvate (100 μM) medium to reveal respiratory dependency on other

279 substrates, we showed that CPT1A–mediated mitochondrial oxidation of endogenous long
280 chain fatty acids (LCFA; etomoxir-inhibited) was similar between genotypes (Figure 4E). Next,
281 we by–passed CPT1A–mediated LCFA transfer, and revealed a marked deficit in respiration
282 stimulated by the medium chain fatty acid octanoate in hepatocytes from *Tst*$^{-/-}$ mice (Figure
283 4F). A similar experiment adding back pyruvate revealed comparable stimulation of
284 respiration between genotypes (Figure S5I). In amino acid free media, combined glutamine–,
285 aspartate– and alanine–stimulated hepatocyte respiration was comparable between
286 genotypes (Figure S5J).

287

288 # Discussion

289 Elevated TST expression in adipose tissue was recently identified as a genetic mechanism
290 driving metabolically protective leanness in mice[35]. Conversely, mice with genetic deletion of
291 *Tst* (*Tst*$^{-/-}$ mice) exhibited impaired glucose tolerance relative to C57BL/6N controls[35]. A key
292 observation from the *Tst*$^{-/-}$ mouse was qualitative evidence for elevated blood sulfide
293 levels[35], which implicated the mitochondrial sulfurtransferase in the breakdown of sulfide for
294 the first time *in vivo*. However, the mechanistic link between *Tst* deficiency and impaired
295 glucose tolerance remained unclear. The *Tst*$^{-/-}$ mice had a subtle adipose tissue phenotype,
296 with comparable fat accumulation upon high fat feeding, suggesting alternate organs as a
297 potential source of impaired glucose homeostasis. Moreover, TST is most highly abundant in
298 the liver, consistent with its role in detoxification of cyanide and related molecules. Indeed,
299 hepatic TST mRNA levels are ~8-fold higher than adipose tissue, with the difference in enzyme
300 activity likely substantially exceeding this, per gram of tissue. Based upon the reported effects
301 of sulfide to increase hepatic glucose production[20,21] and modulate lipid metabolism[22,23], we
302 hypothesised that TST deficiency predominantly drives a diabetogenic state through
303 increased hepatic sulfide exposure. Consistent with this, we found evidence for increased
304 gluconeogenesis, steatosis, elevated plasma VLDL triglycerides and, quantitatively, a 10-fold
305 higher circulating blood sulfide level in *Tst*$^{-/-}$ mice. Unexpectedly, and in spite of the
306 markedly increased circulating sulfide levels, steady-state sulfide level was normal in the liver
307 of *Tst*$^{-/-}$ mice. Moreover, we found evidence for multiple mechanisms for increased, not
308 decreased, hepatic sulfide disposal, reduced downstream sulfide signalling and novel
309 molecular explanations for the apparently diabetogenic phenotype. Our data are consistent
310 with the liver being a major site for sulfide disposal rather than production[32]. Moreover, our

311 data suggest that the liver of *Tst*$^{-/-}$ mice has over-compensated in its response to maximise
312 hepatic sulfide removal, thus engendering detrimental metabolic consequences indirectly.
313 This response is achieved through a combination of distinct compartmentalised cellular
314 responses including increased respiratory sulfide disposal and export of cysteine and GSH and
315 is further evidenced by the reduction of global hepatic protein persulfidation and depletion
316 of sulfide-responsive[49] NRF2 target proteins. Additionally, up-regulation of translation and
317 recruitment of MPST to the mitochondria of *Tst*$^{-/-}$ mice is observed. This response, in face
318 of reduced transcription of *Mpst* due to *Mpst* promoter disruption by the *Tst* null allele,
319 suggests a powerful post-transcriptional cellular sulfide sensing mechanism. Moreover, if
320 MPST is compensating for TST–mediated sulfide disposal in this context, this suggests a
321 subversion of normal MPST function away from sulfide production[50,51 52,53]. Intriguingly, TST
322 expression levels were elevated in the liver of *Mpst*$^{-/-}$ mice, providing further support for an
323 exquisite reciprocal compensatory mechanism between these two enzymes[54].
324 The unexpected finding of normal hepatic sulfide levels in the *Tst*$^{-/-}$ mice led us to discover
325 that the metabolic phenotype we observed was driven by the very mechanisms invoked to
326 maintain sulfide within a normal range rather than sulfide excess *per se*. Several observations
327 were consistent with this. For example, the major amino acid pathways increased in the liver
328 proteome of *Tst*$^{-/-}$ mice were transaminases involved in metabolism of GSH that support
329 increased export of sulfur equivalents as GSH (and cysteine). These same transaminases
330 support gluconeogenesis by redirecting Krebs cycle intermediates[55–57]. In addition,
331 glutathione-S-transferases (GST) that inhibit gluconeogenesis[58] were lower in the liver of *Tst*$^{-}$
332 $^{/-}$ mice. Further, NRF2 activation, which represses gluconeogenesis[59] appears lower in liver
333 of *Tst*$^{-/-}$ mice. The involvement of NRF2 in the *Tst*$^{-/-}$ liver phenotype is further supported by
334 the phenotype of *Nrf2*$^{-/-}$ mice that also exhibited steatohepatitis, in the absence of insulin

335 resistance[60]. However, we note that NRF2 signalling can be complex and dependent upon
336 dietary context; *Nrf2*$^{-/-}$ mice showed improved glucose tolerance after a high–fat diet[61]
337 suggesting any contribution of a NRF2 signalling deficit in the liver of the *Tst*$^{-/-}$ mice changes
338 upon high fat feeding. Beyond gluconeogenesis, we also showed that the hepatocytes of *Tst*$^{-}$
339 $^{/-}$ mice exhibited defective lipid metabolism. Specifically, medium–chain fatty acid (MCFA)
340 oxidation was impaired, associated with selective reduction of protein levels and
341 persulfidation levels of lipid catabolic enzymes. This represents a novel mechanism linking
342 altered sulfide metabolism to lipid oxidation, hepatic lipid accumulation and dyslipidaemia.
343 Consistent with impaired MCFA oxidation defects as a driver, at least in part, of the phenotype
344 of *Tst*$^{-/-}$ mice, steatosis is observed in medium–chain acyl-CoA dehydrogenase (*Mcad*)$^{-/-}$
345 mice[62] and dyslipidemia is found in MCADD deficient humans[63]. The data we present adds to
346 a growing understanding of the link between sulfide regulating genes and nutrient
347 metabolism that has hitherto focussed on the enzymes of sulfide production. Specifically, we
348 provide support for the importance of the sulfide oxidising pathway as a regulator of cellular
349 sulfide exposure. Unexpectedly, the data reveal novel cellular mechanisms that are engaged
350 to homeostatically regulate sulfide disposal and that can impact upon cell energetics and
351 nutrient metabolism.
352 Our findings may have implications for potentially unexpected side effects of sulfide donor
353 therapeutics. In normal mice, *in vivo* sulfide administration for 4 weeks post HFD partially
354 reversed hepatic lipid accumulation invoked by chronic (16 weeks) HFD[22]. No evidence was
355 provided for whether sulfide disposal mechanisms were altered[22]. This efficacious sub-
356 chronic sulfide administration regimen contrasts with our genetic model of chronic sulfide
357 elevation as a driver of dysregulated metabolism and NAFLD. Clearly, the normal mice in the
358 Na_2S administration studies had a fully functional SOP, suggesting the presence of TST is

359 required to achieve the beneficial metabolic effects of Na_2S administration. This is also
360 consistent with the apparently low sulfide signalling status (evidenced by lower
361 persulfidation, NRF2 target protein abundance) in the liver of the *Tst*$^{-/-}$ mice. The benefits
362 of elevated sulfide cannot be realised, perhaps because the major mediator of those effects
363 is missing and the alternate mechanisms invoked do not fully compensate (e.g. MPST) or
364 actively drive aberrant nutrient metabolism. Comparable studies of glucose and lipid
365 metabolism after manipulation of other sulfide regulating genes are limited. However in a
366 contrasting model of reduced sulfide production (*Cth*$^{-/-}$ mice), plasma triglycerides were
367 lowered[23], consistent and opposite to what we observed with the *Tst*$^{-/-}$ mice. The hepatic
368 sulfide disposal status of the *Cth*$^{-/-}$ mouse model is unknown, but our findings predict a
369 suppression of the SOP to spare the limited endogenous sulfide produced. Intriguingly they
370 also predict a knock-on effect on nutrient homeostasis due to reduced metabolic demand of
371 the TST/SOP axis. A more direct model informing on the effects of impairment of the sulfide
372 disposal pathway is deficiency of the key mitochondrial SOP enzyme ETHE1. *Ethe1*$^{-/-}$ mice
373 suffer fatal sulfide toxicity[30] and therefore comparable metabolic studies are lacking.
374 However, one notable observation is that *Ethe1*$^{-/-}$ mice have an apparently 10-fold higher
375 liver sulfide exposure than control mice[30], in contrast to the normalised hepatic sulfide levels
376 of *Tst*$^{-/-}$ mice. Circulating sulfide levels were not reported for comparison, but the
377 presumably relatively lower systemic sulfide levels of *Tst*$^{-/-}$ mice appear to have permitted
378 an effective homeostatic sulfide disposal response in the liver to avoid toxicity, albeit with a
379 metabolic cost. Consequently, the liver of *Tst*$^{-/-}$ mice has a distinct functional and proteomic
380 profile to that of the *Ethe1*$^{-/-}$ mice. For example, in the liver of *Tst*$^{-/-}$ and *Ethe1*$^{-/-}$ mice[64],
381 proteins of the glutathione–S–transferase Mu type (GSTM) and peroxiredoxin (PRDX) families
382 were altered, but sometimes in the opposite direction or with alteration of distinct protein

383 sub-classes. A notable difference is also observed in amino acid metabolism. The liver of
384 *Ethe1*$^{-/-}$ mice exhibited increased expression of enzymes of branched chain amino acid
385 metabolism[64], distinct from the predominantly glutathione–related amino acid pathways that
386 are increased in liver of *Tst*$^{-/-}$ mice. Beyond sulfide, TST may also have distinct cellular roles
387 that affect metabolism such as mitoribosomal synthesis, ROS attenuation and modulation of
388 mitochondrial iron-sulfur clusters[65–69].
389 Given the pro-diabetogenic liver phenotype in *Tst*$^{-/-}$ mice, its was surprising that insulin
390 signalling in the liver appeared normal, and peripheral insulin sensitivity was increased. There
391 are precedents for increased hepatic glucose production independent of insulin resistance, as
392 found in the *Nrf2*$^{-/-}$ mice[60] and as driven by the transcription factor ChREBP[70,71]. There is
393 also evidence to support insulin–sensitising effects of sulfide administration *in vivo* in mice
394 and rats[72–74], consistent with a sulfide–mediated insulin–sensitisation of non-hepatic tissues
395 in *Tst*$^{-/-}$ mice. Higher circulating GSH in *Tst*$^{-/-}$ mice may also promote peripheral insulin–
396 sensitisation[75,76]. Clearly, the net balance of glucose production from the liver and its
397 peripheral disposal remains abnormal in *Tst*$^{-/-}$ mice. Indeed, the baseline metabolic
398 phenotype of *Tst*$^{-/-}$ mice resembles in many ways that of a normal mouse fed a HFD. Thus
399 we expected to gain insight into conserved pro-diabetogenic mechanisms from the overlap
400 between the liver proteome of *Tst*$^{-/-}$ mice and that of HFD-fed C57BL/6J mice. However,
401 upon closer inspection this was not entirely the case, with some lipid metabolism and
402 peroxisomal proteins changing in the opposite direction to those observed in HFD–fed
403 C57BL/6J mice. Unlike a HFD state, which is associated with dominant hepatic insulin
404 resistance, the increased hepatic glucose production in ND-fed *Tst*$^{-/-}$ mice appears to be a
405 result of their over-compensated sulfide-removal response.

406 Sulfide donor therapeutics were proposed as a clinical strategy for improving cardiovascular
407 health[27,77,78]. Elevated endogenous sulfide was also implicated in the beneficial metabolic
408 effects of caloric restriction[11,79–83]. Our results suggest that chronic sulfide elevation may have
409 unintended detrimental consequences, driving liver glucose production and fat accumulation
410 to undesirable levels. This caveat may be fortunately limited to cases where SOP proteins are
411 compromised through rare genetic effects – such as TST variants[84,85]. More broadly, a number
412 of drugs or supplements are known to increase cyanide, which may dominantly inhibit TST
413 activity and result in secondary sulfide overexposure. These include nitroprusside[86] and
414 amygdalin[87,88]. Indeed the TST metabolite thiosulfate is commonly co-administered with
415 nitroprusside to prevent cyanide toxicity[89]. Furthermore, dietary and environmental exposure
416 to cyanogenic compounds[90], e.g. smoking[91] or cyanogenic diets[92] may interfere with normal
417 TST function and could lead to increased sensitivity to sulfide therapeutics. In contrast, we
418 have shown that administration of the TST substrate thiosulfate can ameliorate diabetes[35]
419 further underlining the potential utility of targeting the SOP in metabolic disease. As with all
420 therapeutic strategies, a careful cost-benefit analysis is required. A comparable case of
421 relevance are the statins, one of the most potent and widely used drugs to prevent
422 atherosclerosis, which also carry a higher risk for diabetes[93]. The full impact of TST
423 manipulation on opposing metabolic pathways requires further study. Our current study
424 sheds light on the underlying hepatic mechanisms invoked for sulfide disposal that are
425 relevant to current sulfide–donor strategines and may inform on routes to reduce their
426 potential metabolic side-effects.
427
428
429

Methods

The methods for all data and work presented in this manuscript is provided as supplementary information.

Author Contributions

N.M.M. and R.N.C conceived experiments. R.N.C., M.T.G.G, M. B.-L., A. M.-C., M.L., V.V., B.E., T. LeB., M.B., S.H., S.D., N.H., C. Mc F., A.T., N. F., T.G., performed experiments. R.N.C., M. B.-L., P.F., V.V., T. LeB., N.H., T.S., F.B., T.G., R.C.H., B.S., G.G., A.J.F., C.S., R.B. and N.M.M. analysed and interpreted data and commented on the manuscript. K.H.A., S.S. generated reagents. C.McM. and R.C.H. generated reagents. R.N.C. and N.M.M. wrote the manuscript.

Acknowledgements

This work was funded by a Wellcome Trust New Investigator Award to NMM (100981/Z/13/Z) and Diabetes UK grant (17/0005697). RCH was funded by a Medical Research Council Discovery Award (MC-PC-15076). We would like to thank Professor Ken Olsen and Eric DeLeon (Notre Dame) for advice establishing sulfide measurement by probe.

460 # References

461 1. World Health Organisation. Global report on diabetes.
462 2016;https://www.who.int/publications-detail/global-report-on-diabetes
463 2. Lewis GF, Carpentier A, Adeli K, Giacca A. Disordered fat storage and mobilization in
464 the pathogenesis of insulin resistance and type 2 diabetes. *Endocr Rev*.
465 2002;23(2):201-229. doi:10.1210/edrv.23.2.0461
466 3. Consoli A, Nurjhan N, Capani F, Gerich J. Predominant role of gluconeogenesis in
467 increased hepatic glucose production in NIDDM. *Diabetes*. 1989;38(5):550-557.
468 doi:10.2337/diab.38.5.550
469 4. Caron S, et al. Transcriptional activation of apolipoprotein CIII expression by glucose
470 may contribute to diabetic dyslipidemia. *Arterioscler Thromb Vasc Biol*.
471 2011;31(3):513-519. doi:10.1161/ATVBAHA.110.220723
472 5. Abe K, Kimura H. The possible role of hydrogen sulfide as an endogenous
473 neuromodulator. *J Neurosci*. 1996;16(3):1066-1071.
474 doi:10.1523/JNEUROSCI.16-03-01066
475 6. Wang R. Physiological Implications of Hydrogen Sulfide: A Whiff Exploration That
476 Blossomed. *Physiol Rev*. 2012;92(2):791-896. doi:10.1152/physrev.00017.2011
477 7. Mishanina T V., Libiad M, Banerjee R. Biogenesis of reactive sulfur species for
478 signaling by hydrogen sulfide oxidation pathways. *Nat Chem Biol*.
479 2015;11(7):457-464. doi:10.1038/nchembio.1834
480 8. Filipovic MR, Zivanovic J, Alvarez B, Banerjee R. Chemical Biology of H_2S Signaling
481 through Persulfidation. *Chem Rev*. 2018;118(3):1253-1337.
482 doi:10.1021/acs.chemrev.7b00205
483 9. Desai KM, Chang T, Untereiner A, Wu L. Hydrogen sulfide and the metabolic

484 syndrome. *Expert Rev Clin Pharmacol*. 2011;4(1):63-73. doi:10.1586/ecp.10.133
485 10. Szabo C. Roles of Hydrogen Sulfide in the Pathogenesis of Diabetes Mellitus and Its
486 Complications. *Antioxid Redox Signal*. 2011;17(1):68-80. doi:10.1089/ars.2011.4451
487 11. Hine C, et al. Endogenous hydrogen sulfide production is essential for dietary
488 restriction benefits. *Cell*. 2015;160(1-2):132-44. doi:10.1016/j.cell.2014.11.048
489 12. Carter RN, Morton NM. Cysteine and hydrogen sulphide in the regulation of
490 metabolism: Insights from genetics and pharmacology. *J Pathol*. 2016;238(2):321-332.
491 doi:10.1002/path.4659
492 13. Chen X, Jhee KH, Kruger WD. Production of the neuromodulator H2S by
493 cystathionine beta-synthase via the condensation of cysteine and homocysteine. *J*
494 *Biol Chem*. 2004;279(50):52082-6. doi:10.1074/jbc.C400481200
495 14. Singh S, Padovani D, Leslie RA, Chiku T, Banerjee R. Relative contributions of
496 cystathionine beta-synthase and gamma-cystathionase to H2S biogenesis via
497 alternative trans-sulfuration reactions. *J Biol Chem*. 2009;284(33):22457-66.
498 doi:10.1074/jbc.M109.010868
499 15. Shibuya N, et al. 3-Mercaptopyruvate sulfurtransferase produces hydrogen sulfide
500 and bound sulfane sulfur in the brain. *Antioxid Redox Signal*. 2009;11(4):703-14.
501 doi:10.1089/ars.2008.2253
502 16. Mikami Y, Shibuya N, Kimura Y, Nagahara N, Ogasawara Y, Kimura H. Thioredoxin and
503 dihydrolipoic acid are required for 3-mercaptopyruvate sulfurtransferase to produce
504 hydrogen sulfide. *Biochem J*. 2011;439(3):479-85. doi:10.1042/BJ20110841
505 17. Yadav PK, Yamada K, Chiku T, Koutmos M, Banerjee R. Structure and kinetic analysis
506 of H2S production by human mercaptopyruvate sulfurtransferase. *J Biol Chem*.
507 2013;288(27):20002-13. doi:10.1074/jbc.M113.466177

508 18. Wedmann R, et al. Improved tag-switch method reveals that thioredoxin acts as
509 depersulfidase and controls the intracellular levels of protein persulfidation. *Chem*
510 *Sci*. 2016;7(5):3414-3426. doi:10.1039/c5sc04818d
511 19. Mani S, Cao W, Wu L, Wang R. Hydrogen sulfide and the liver. *Nitric Oxide - Biol*
512 *Chem*. 2014;312(3):H406-H414. doi:10.1016/j.niox.2014.02.006
513 20. Pichette J, Gagnon J. Implications of Hydrogen Sulfide in Glucose Regulation: How
514 H2S Can Alter Glucose Homeostasis through Metabolic Hormones. *Oxid Med Cell*
515 *Longev*. 2016;2016:3285074. doi:10.1155/2016/3285074
516 21. Zhang L, Yang G, Untereiner A, Ju Y, Wu L, Wang R. Hydrogen sulfide impairs glucose
517 utilization and increases gluconeogenesis in hepatocytes. *Endocrinology*.
518 2013;154(1):114-126. doi:10.1210/en.2012-1658
519 22. Wu D, et al. Exogenous hydrogen sulfide mitigates the fatty liver in obese mice
520 through improving lipid metabolism and antioxidant potential. *Med Gas Res*.
521 2015;5(1):1-8. doi:10.1186/s13618-014-0022-y
522 23. Mani S, et al. Decreased endogenous production of hydrogen sulfide accelerates
523 atherosclerosis. *Circulation*. 2013;127(25):2523-2534.
524 doi:10.1161/CIRCULATIONAHA.113.002208
525 24. Distrutti E, et al. The methionine connection: Homocysteine and hydrogen sulfide
526 exert opposite effects on hepatic microcirculation in rats. *Hepatology*.
527 2008;47(2):659-667. doi:10.1002/hep.22037
528 25. Fiorucci S, et al. The third gas: H2S regulates perfusion pressure in both the isolated
529 and perfused normal rat liver and in cirrhosis. *Hepatology*. 2005;42(3):539-548.
530 doi:10.1002/hep.20817
531 26. Sestito S, Nesi G, Pi R, Macchia M, Rapposelli S. Hydrogen Sulfide: A Worthwhile Tool

532 in the Design of New Multitarget Drugs. *Front Chem*. 2017;5:72.
533 doi:10.3389/fchem.2017.00072
534 27. Whiteman M, Le Trionnaire S, Chopra M, Fox B, Whatmore J. Emerging role of
535 hydrogen sulfide in health and disease: critical appraisal of biomarkers and
536 pharmacological tools. *Clin Sci*. 2011;121(11):459-488. doi:10.1042/cs20110267
537 28. Libiad M, et al. Thiosulfate Sulfurtransferase like Domain Containing 1 Protein
538 Interacts with Thioredoxin. *J Biol Chem*. January 2018;293(8):2675-2686.
539 doi:10.1074/jbc.RA117.000826
540 29. Reiffenstein R. Toxicology Of Hydrogen Sulfide. *Annu Rev Pharmacol Toxicol*.
541 1992;32(1):109-134. doi:10.1146/annurev.pharmtox.32.1.109
542 30. Tiranti V, et al. Loss of ETHE1, a mitochondrial dioxygenase, causes fatal sulfide
543 toxicity in ethylmalonic encephalopathy. *Nat Med*. 2009;15(2):200-205.
544 doi:10.1038/nm.1907
545 31. Hildebrandt TM, Grieshaber MK. Three enzymatic activities catalyze the oxidation of
546 sulfide to thiosulfate in mammalian and invertebrate mitochondria. *FEBS J*.
547 2008;275(13):3352-3361. doi:10.1111/j.1742-4658.2008.06482.x
548 32. Norris EJ, Culberson CR, Narasimhan S, Clemens MG. The liver as a central regulator
549 of hydrogen sulfide. *Shock*. 2011;36(3):242-50. doi:10.1097/SHK.0b013e3182252ee7
550 33. Jackson MR, Melideo SL, Jorns MS. Human sulfide:Quinone oxidoreductase catalyzes
551 the first step in hydrogen sulfide metabolism and produces a sulfane sulfur
552 metabolite. *Biochemistry*. 2012;51(34):6804-15. doi:10.1021/bi300778t
553 34. Libiad M, Yadav PK, Vitvitsky V, Martinov M, Banerjee R. Organization of the human
554 mitochondrial hydrogen sulfide oxidation pathway. *J Biol Chem*.
555 2014;289(45):30901-10. doi:10.1074/jbc.M114.602664

556 35. Morton NM, et al. Genetic identification of thiosulfate sulfurtransferase as an
557 adipocyte-expressed antidiabetic target in mice selected for leanness. *Nat Med*.
558 2016;22(7):771-9. doi:10.1038/nm.4115
559 36. Gero D, et al. The novel mitochondria-targeted hydrogen sulfide (H2S) donors AP123
560 and AP39 protect against hyperglycemic injury in microvascular endothelial cells in
561 vitro. *Pharmacol Res*. 2016;113:186-198. doi: 10.1016/j.phrs.2016.08.019
562 37. Karwi QG, Bice JS, Baxter GF. Pre- and postconditioning the heart with hydrogen
563 sulfide (H2S) against ischemia/reperfusion injury in vivo: a systematic review and
564 meta-analysis. *Basic Res Cardiol*. 2018;113(1):6. doi:10.1007/s00395-017-0664-8
565 38. Mason TM. The role of factors that regulate the synthesis and secretion of very-low-
566 density lipoprotein by hepatocytes. *Crit Rev Clin Lab Sci*. 1998;35(6):461-487.
567 doi:10.1080/10408369891234246
568 39. Vitvitsky V, Yadav PK, Kurthen A, Banerjee R. Sulfide oxidation by a noncanonical
569 pathway in red blood cells generates thiosulfate and polysulfides. *J Biol Chem*.
570 2015;290(13):8310-8320. doi:10.1074/jbc.M115.639831
571 40. Vitvitsky V, Yadav PK, An S, Seravalli J, Cho US, Banerjee R. Structural and mechanistic
572 insights into hemoglobincatalyzed hydrogen sulfide oxidation and the fate of
573 polysulfide products. *J Biol Chem*. 2017;292(13):5584-5592.
574 doi:10.1074/jbc.M117.774943
575 41. Banerjee R, Chiku T, Kabil O, Libiad M, Motl N, Yadav PK. *Assay Methods for H2S*
576 *Biogenesis and Catabolism Enzymes*. Vol 554. Academic Press Inc.; 2015:189-200.
577 doi:10.1016/bs.mie.2014.11.016
578 42. Singha S, et al. Toward a selective, sensitive, fast-responsive, and biocompatible two-
579 photon probe for hydrogen sulfide in live cells. *Anal Chem*. 2015;87(2):1188-1195.

580 doi:10.1021/ac503806w

581 43. Arndt S, et al. Assessment of H2S in vivo using the newly developed mitochondria-
582 targeted mass spectrometry probe MitoA. *J Biol Chem*. 2017;292(19):7761-7773.
583 doi:10.1074/jbc.M117.784678

584 44. Krishnan N, Fu C, Pappin DJ, Tonks NK. H2S-Induced Sulfhydration of the Phosphatase
585 PTP1B and Its Role in the Endoplasmic Reticulum Stress Response. *Sci Signal*.
586 2011;4:ra86. doi:10.1126/scisignal.2002329

587 45. Kabil O, Motl N, Banerjee R. H2S and its role in redox signaling. *Biochim Biophys Acta -*
588 *Proteins Proteomics*. 2014;1844(8):1355-1366. doi:10.1016/j.bbapap.2014.01.002

589 46. Koike S, Nishimoto S, Ogasawara Y. Cysteine persulfides and polysulfides produced by
590 exchange reactions with H2S protect SH-SY5Y cells from methylglyoxal-induced
591 toxicity through Nrf2 activation. *Redox Biol*. 2017;12:530-539.
592 doi:10.1016/j.redox.2017.03.020

593 47. Nagahara N. Catalytic site cysteines of thiol enzyme: eulfurtransferases. *J Amino*
594 *Acids*. 2011;2011:709404. doi:10.4061/2011/709404

595 48. Xie L, et al. Hydrogen sulfide induces Keap1 S-sulfhydration and suppresses diabetes-
596 accelerated atherosclerosis via Nrf2 activation. *Diabetes*. 2016;65(10):3171-3184.
597 doi:10.2337/db16-0020

598 49. Yang G, et al. Hydrogen sulfide protects against cellular senescence via s-
599 sulfhydration of keap1 and activation of Nrf2. *Antioxidants Redox Signal*.
600 2013;18(15):1906-1919. doi:10.1089/ars.2012.4645

601 50. Módis K, Coletta C, Erdélyi K, Papapetropoulos A, Szabo C. Intramitochondrial
602 hydrogen sulfide production by 3-mercaptopyruvate sulfurtransferase maintains
603 mitochondrial electron flow and supports cellular bioenergetics. *FASEB J*.

604 2013;27(2):601-11. doi:10.1096/fj.12-216507

605 51. Szabo C, et al. Regulation of mitochondrial bioenergetic function by hydrogen sulfide.
606 Part I. Biochemical and physiological mechanisms. *Br J Pharmacol*.
607 2014;171(8):2099-122. doi:10.1111/bph.12369

608 52. Nagahara N. Multiple role of 3-mercaptopyruvate sulfurtransferase: antioxidative
609 function, H2S and polysulfide production and possible SOx production. *Br J*
610 *Pharmacol*. 2018;175(4):577-589. doi:10.1111/bph.14100

611 53. Kimura Y, Koike S, Shibuya N, Lefer D, Ogasawara Y, Kimura H. 3-Mercaptopyruvate
612 sulfurtransferase produces potential redox regulators cysteine- and glutathione-
613 persulfide (Cys-SSH and GSSH) together with signaling molecules H2S2, H2S3 and H2S.
614 *Sci Rep*. 2017;7(1):1-14. doi:10.1038/s41598-017-11004-7

615 54. Nagahara N, Tanaka M, Tanaka Y, Ito T. Novel Characterization of Antioxidant
616 Enzyme, 3-Mercaptopyruvate Sulfurtransferase-Knockout Mice: Overexpression of
617 the Evolutionarily-Related Enzyme Rhodanese. *Antioxidants*. 2019;8(5):116.
618 doi:10.3390/antiox8050116

619 55. Rui L. Energy metabolism in the liver. *Compr Physiol*. 2014;4(1):177-197.
620 doi:10.1002/cphy.c130024

621 56. Qian K, Zhong S, Xie K, Yu D, Yang R, Gong DW. Hepatic ALT isoenzymes are elevated
622 in gluconeogenic conditions including diabetes and suppressed by insulin at the
623 protein level. *Diabetes Metab Res Rev*. 2015;31(6):562-571. doi:10.1002/dmrr.2655

624 57. Sookoian S, et al. Serum aminotransferases in nonalcoholic fatty liver disease are a
625 signature of liver metabolic perturbations at the amino acid and Krebs cycle level. *Am*
626 *J Clin Nutr*. 2016;103(2):422-434. doi:10.3945/ajcn.115.118695

627 58. Ghosh Dastidar S, et al. Glutathione S -transferase P deficiency induces glucose

628 intolerance via JNK-dependent enhancement of hepatic gluconeogenesis. *Am J*
629 *Physiol Metab*. 2018;315(5):E1005-E1018. doi:10.1152/ajpendo.00345.2017
630 59. Slocum SL, et al. Keap1/Nrf2 pathway activation leads to a repressed hepatic
631 gluconeogenic and lipogenic program in mice on a high-fat diet. *Arch Biochem*
632 *Biophys*. 2016;591:57-65. doi:10.1016/j.abb.2015.11.040
633 60. Meakin PJ, et al. Susceptibility of Nrf2-Null Mice to Steatohepatitis and Cirrhosis upon
634 Consumption of a High-Fat Diet Is Associated with Oxidative Stress, Perturbation of
635 the Unfolded Protein Response, and Disturbance in the Expression of Metabolic
636 Enzymes but Not with Insulin Resistance. *Mol Cell Biol*. 2014;34(17):3305-3320.
637 doi:10.1128/mcb.00677-14
638 61. Zhang YKJ, Wu KC, Liu J, Klaassen CD. Nrf2 deficiency improves glucose tolerance in
639 mice fed a high-fat diet. *Toxicol Appl Pharmacol*. 2012;264(3):305-314.
640 doi:10.1016/j.taap.2012.09.014
641 62. Tolwani RJ, et al. Medium-chain acyl-CoA dehydrogenase deficiency in gene-targeted
642 mice. *PLoS Genet*. 2005;1(2):0205-0212. doi:10.1371/journal.pgen.0010023
643 63. Onkenhout W, Venizelos V, Van Der Poet PFH, Van Den Heuvel MPM, Poorthuis BJ.
644 Identification and quantification of intermediates of unsaturated fatty acid
645 metabolism in plasma of patients with fatty acid oxidation disorders. *Clin Chem*.
646 1995;41(10):1467-74. PMID: 7586519
647 64. Hildebrandt TM, Di Meo I, Zeviani M, Viscomi C, Braun H. Proteome adaptations in
648 Ethe1-deficient mice indicate a role in lipid catabolism and cytoskeleton organization
649 via post-translational protein modifications. *Biosci Rep*. 2013;33(4):575-584.
650 doi:10.1042/bsr20130051
651 65. Bonomi F, Pagani S, Cerletti P, Cannella C. Rhodanese-Mediated Sulfur Transfer to

652 Succinate Dehydrogenase. *Eur J Biochem*. 1977;72(1):17-24.
653 doi:10.1111/j.1432-1033.1977.tb11219.x
654 66. Pagani S, Galante YM. Interaction of rhodanese with mitochondrial NADH
655 dehydrogenase. *Biochim Biophys Acta*. 1983;742(2):278-84.
656 doi:10.1016/0167-4838(83)90312-6
657 67. Nandi DL, Westley J. Reduced thioredoxin as a sulfur-acceptor substrate for
658 rhodanese. *Int J Biochem Cell Biol*. 1998;30(9):973-7.
659 doi:10.1016/S1357-2725(98)00050-8
660 68. Nandi DL, Horowitz PM, Westley J. Rhodanese as a thioredoxin oxidase. *Int J Biochem*
661 *Cell Biol*. 2000;32(4):465-473. doi:10.1016/S1357-2725(99)00035-7
662 69. Smirnov A, et al. Mitochondrial enzyme rhodanese is essential for 5S ribosomal RNA
663 import into human mitochondria. *J Biol Chem*. 2010;285(40):30792-30803.
664 doi:10.1074/jbc.M110.151183
665 70. Uyeda K, Repa JJ. Carbohydrate response element binding protein, ChREBP, a
666 transcription factor coupling hepatic glucose utilization and lipid synthesis. *Cell*
667 *Metab*. 2006;4(2):107-110. doi:10.1016/j.cmet.2006.06.008
668 71. Kim MS, et al. ChREBP regulates fructose-induced glucose production independently
669 of insulin signaling. *J Clin Invest*. 2016;126(11):4372-4386. doi:10.1172/JCI81993
670 72. Xue R, et al. Hydrogen Sulfide Treatment Promotes Glucose Uptake by Increasing
671 Insulin Receptor Sensitivity and Ameliorates Kidney Lesions in Type 2 Diabetes.
672 *Antioxid Redox Signal*. 2013;19(1):5-23. doi:10.1089/ars.2012.5024
673 73. Feng X, Chen Y, Zhao J, Tang C, Jiang Z, Geng B. Hydrogen sulfide from adipose tissue
674 is a novel insulin resistance regulator. *Biochem Biophys Res Commun*.
675 2009;380(1):153-9. doi:10.1016/j.bbrc.2009.01.059

676 74. Geng B, et al. Increase or Decrease Hydrogen Sulfide Exert Opposite Lipolysis, but
677 Reduce Global Insulin Resistance in High Fatty Diet Induced Obese Mice. *PLoS One*.
678 2013;8(9):e73892. doi:10.1371/journal.pone.0073892
679 75. Lutchmansingh FK, et al. Glutathione metabolism in type 2 diabetes and its
680 relationship with microvascular complications and glycemia. *PLoS One*.
681 2018;13(6):e0198626. doi:10.1371/journal.pone.0198626
682 76. Jain SK, Micinski D, Huning L, Kahlon G, Bass PF, Levine SN. Vitamin D and L-cysteine
683 levels correlate positively with GSH and negatively with insulin resistance levels in the
684 blood of type 2 diabetic patients. *Eur J Clin Nutr*. 2014;68(10):1148-1153.
685 doi:10.1038/ejcn.2014.114
686 77. Zhang L, et al. Hydrogen sulfide (H2S)-releasing compounds: Therapeutic potential in
687 cardiovascular diseases. *Front Pharmacol*. 2018;9:1066.
688 doi:10.3389/fphar.2018.01066
689 78. Szabó G, et al. Cardioprotective effects of hydrogen sulfide. *Nitric Oxide.*
690 2011;25(2):201-210. doi:10.1016/j.niox.2010.11.001
691 79. Miller RA, Buehner G, Chang Y, Harper JM, Sigler R, Smith-Wheelock M. Methionine-
692 deficient diet extends mouse lifespan, slows immune and lens aging, alters glucose,
693 T4, IGF-I and insulin levels, and increases hepatocyte MIF levels and stress resistance.
694 *Aging Cell*. 2005;4(3):119-25. doi:10.1111/j.1474-9726.2005.00152.x
695 80. Lee BC, Kaya A, Gladyshev VN. Methionine restriction and life-span control. *Ann N Y*
696 *Acad Sci*. 2016;1363:116-24. doi:10.1111/nyas.12973
697 81. Shimokawa I, et al. The life-extending effect of dietary restriction requires Foxo3 in
698 mice. *Aging Cell*. 2015;14(4):707-9 doi:10.1111/acel.12340
699 82. Hine C, et al. Hypothalamic-pituitary axis regulates hydrogen sulfide production. *Cell*

700 *Metab*. 2017;25(6):1320-1333 doi:10.1016/j.cmet.2017.05.003

701 83. Hine C, Zhu Y, Hollenberg AN, Mitchell JR. Dietary and endocrine regulation of
702 endogenous hydrogen sulfide production: implications for longevity. *Antioxid Redox*
703 *Signal*. 2018;28(16):1483-1502. doi:10.1089/ars.2017.7434

704 84. Libiad M, Sriraman A, Banerjee R. Polymorphic variants of human rhodanese exhibit
705 differences in thermal stability and sulfur transfer kinetics. *J Biol Chem*.
706 2015;290(39):23579-88 doi:10.1074/jbc.M115.675694

707 85. Billaut-Laden I, et al. Evidence for a functional genetic polymorphism of the human
708 thiosulfate sulfurtransferase (Rhodanese), a cyanide and H2S detoxification enzyme.
709 *Toxicology*. 2006;225(1):1-11. doi:10.1016/j.tox.2006.04.054

710 86. Morris AA, et al. Thiocyanate Accumulation in Critically Ill Patients Receiving
711 Nitroprusside Infusions. *J Intensive Care Med*. 2017;32(9):547-553.
712 doi:10.1177/0885066616657004

713 87. Bromley J, Hughes BGM, Leong DCS, Buckley NA. Life-threatening interaction
714 between complementary medicines: Cyanide toxicity following ingestion of
715 amygdalin and vitamin C. *Ann Pharmacother*. 2005;39(9):1566-1569.
716 doi:10.1345/aph.1E634

717 88. O'Brien B, Quigg C, Leong T. Severe Cyanide Toxicity from "Vitamin Supplements." *Eur*
718 *J Emerg Med*. 2005;12(5):257-8. doi:10.1097/00063110-200510000-00014

719 89. Curry SC, Carlton MW, Raschke RA. Prevention of fetal and maternal cyanide toxicity
720 from nitroprusside with coinfusion of sodium thiosulfate in gravid ewes. *Anesth*
721 *Analg*. 1997;84(5):1121-1126. doi:10.1213/00000539-199705000-00031

722 90. Petrova F. Hydrogen cyanide and cyanides : human health aspects. 2004;CICAD;61
723 https://www.who.int/ipcs/publications/cicad/en/cicad61.pdf?ua=1

91. Vinnakota C V, et al. Comparison of cyanide exposure markers in the biofluids of smokers and non-smokers. *Biomarkers*. 2012;17(7):625-633. doi:10.3109/1354750X.2012.709880

92. Kashala-Abotnes E, Okitundu D, Mumba D, Boivin MJ, Tylleskär T, Tshala-Katumbay D. Konzo: a distinct neurological disease associated with food (cassava) cyanogenic poisoning. *Brain Res Bull*. 2019;145:87-91. doi:10.1016/j.brainresbull.2018.07.001

93. Swerdlow DI, et al. HMG-coenzyme A reductase inhibition, type 2 diabetes, and bodyweight: Evidence from genetic analysis and randomised trials. *Lancet*. 2015;385(9965):351-361. doi:10.1016/S0140-6736(14)61183-1

Figures and Legends

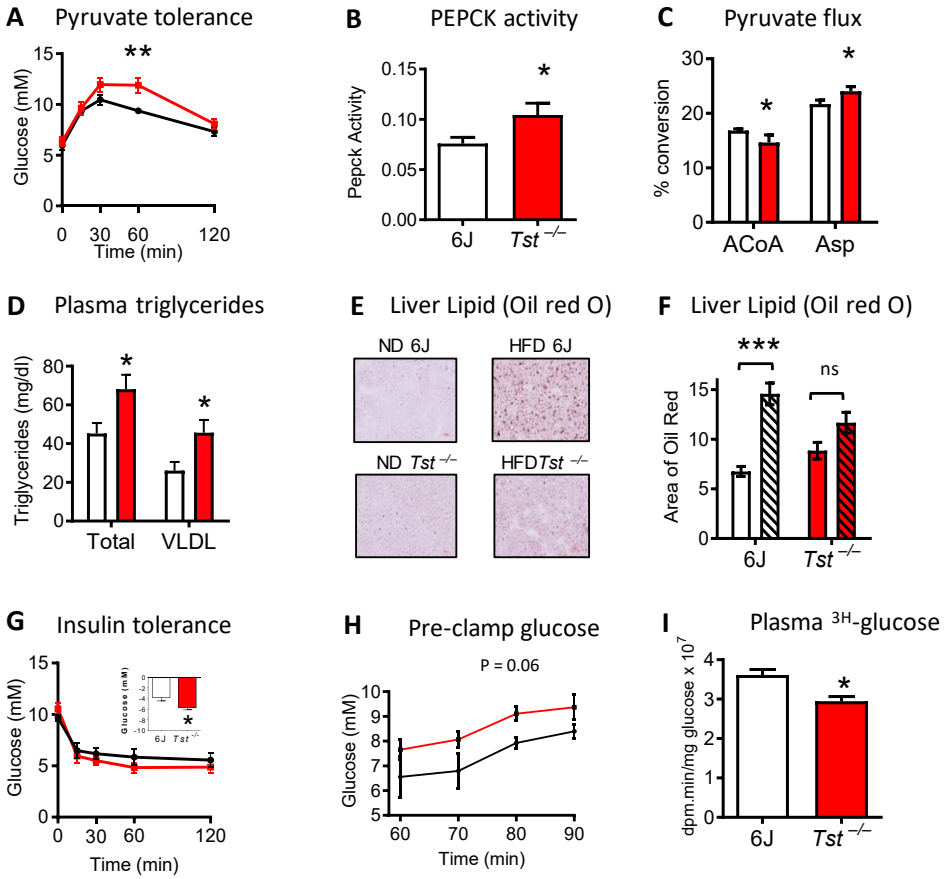

Figure 1. *Tst* deletion results in impaired glucose and lipid metabolism. (**A**) Plasma glucose over 120 minutes, following pyruvate (i.p., 1.5mg/g) administration in overnight fasted C57Bl/6J (black line, n = 9) and *Tst*$^{-/-}$ (red line, n = 8) normal diet-fed mice. (**B**) Extinction of NADH measured by absorbance at 340nm, coupled to PEPCK activity from liver homogenates taken from C57Bl/6J (white bar, n = 6) and *Tst*$^{-/-}$ (red bar, n = 6) normal diet-fed mice. (**C**) Production of ^{13}C (M+2) acetyl-CoA and ^{13}C (M+3) aspartate generated from 3-carbon labelled ^{13}C (M+3) pyruvate, expressed as a percentage of the total amount of detected metabolite, in primary hepatocytes from C57Bl/6J (white bars, n = 6) and *Tst*$^{-/-}$ (red bars, n = 5) normal diet-fed mice. (**D**) HPLC quantified total and VLDL plasma triglyceride in 4 hour fasted C57Bl/6J (white bar, n = 6), and *Tst*$^{-/-}$ (red bar, n = 6) normal diet-fed mice. (**E**) Representative light microscopic images of fixed liver stained with Oil-Red O from normal diet-fed (ND) or high fat diet-fed (HFD) C57Bl/6J and *Tst*$^{-/-}$ mice. (**F**) Analysis of the area of red staining (Oil Red O) after thresholding, using Image J, from normal diet-fed (no pattern, n = 3-4/genotype) or high fat diet-fed (hatched pattern, n = 4-5/genotype) C57Bl/6J (white bars) and *Tst*$^{-/-}$ (red bars) mice. (**G**) Plasma glucose over 120 minutes following insulin (i.p., 1mU/g) administration in 4 hour fasted C57Bl/6J (black line, n = 8) and *Tst*$^{-/-}$(red line, n = 7) normal diet-fed mice. Inset; Reduction in plasma glucose from baseline levels 60 minutes after the injection of insulin. (**H**) Blood glucose during the pre-clamp phase of the hyperinsulinemic, euglycaemic clamp from C57Bl/6J (white, n = 3), and *Tst*$^{-/-}$ (red, n = 6) normal diet-fed mice. Significance is reported from area under curve analysis. (**I**) Mean integrated radioactive glucose (inversely related to whole body glucose uptake) during a hyperinsulinemic, euglycaemic clamp from normal diet fed C57Bl/6J control (white, n = 3), and *Tst*$^{-/-}$ (red, n = 6) mice. Data are represented as mean ±SEM. Significance was calculated using repeated measures ANOVA (**A**,**G**) 2-WAY ANOVA (**C**,**F**) or unpaired two-tailed student's t-test (**B**,**D**,**H**,**I**) * P < 0.05, ** P < 0.01. For (**C**) the 2-WAY ANOVA revealed no overall effect of genotype, however a significant interaction between metabolite and genotype was found. The * on the histogram represents this interaction. For (**F**) no main genotype effect was found, but a significant effect of diet, and an interaction were found. Post Hoc analysis using Sidaks' multiple comparison test show an effect of diet on the 6J controls (***), whereas no effect of diet is found on the *Tst*$^{-/-}$.

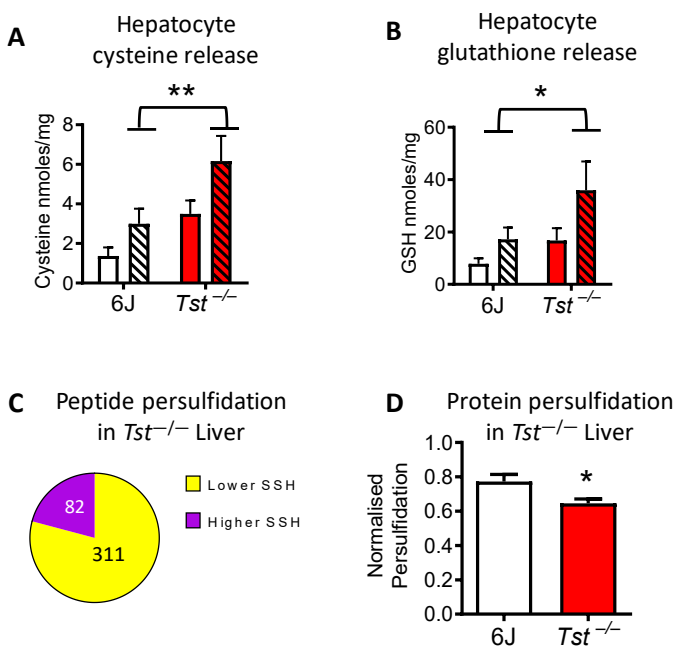

Figure 2. *Tst* deletion results in increased hepatic sulfur excretion and a reduction of protein persulfidation. (**A**) Cysteine concentrations (MBB-HPLC) in the media incubated with primary hepatocytes in the presence (hatched pattern) or absence (no pattern) of 1mM methionine, from C57Bl/6J (white bars, n = 4/treatment) and *Tst*$^{-/-}$ (red bars, n = 4/treatment) mice. (**B**) Glutathione concentrations (MBB-HPLC) in the media incubated with primary hepatocytes in the presence (hatched pattern) or absence (no pattern) of 1mM methionine, from C57Bl/6J (white bars, n = 4/treatment) and *Tst*$^{-/-}$ (red bars, n = 4/treatment) mice. (**C**) Pie chart depicting the proportion of liver peptides that are significantly higher (82 peptides, purple space) or lower (311 peptides, yellow space), in their persulfidation rate in the *Tst*$^{-/-}$ (n = 3) relative to C57Bl/6J (n = 3) mice. (**D**) Total DTT-released cysteine-persulfidated liver protein as measured by REVERT total protein stain following western blotting, normalised to the total input protein of the sample from *Tst*$^{-/-}$ (red bar, n = 4) and C57Bl/6J (white bar, n = 4) mice. Data with error bars are represented as mean ±SEM. Significance was calculated using 2-WAY ANOVA (**A**, **B**) or student's t-test (**D**), * $P < 0.05$, ** $P < 0.01$. For (**A**) and (**B**) the 2-WAY ANOVA reveals a main effect of genotype, indicated by * or ** on the histogram. A significant effect of methionine was also found for both (**A**) and (**B**) not indicated on the histogram. For (**C**) peptides were selected as being significant at a P-diff of 0.95 or greater.

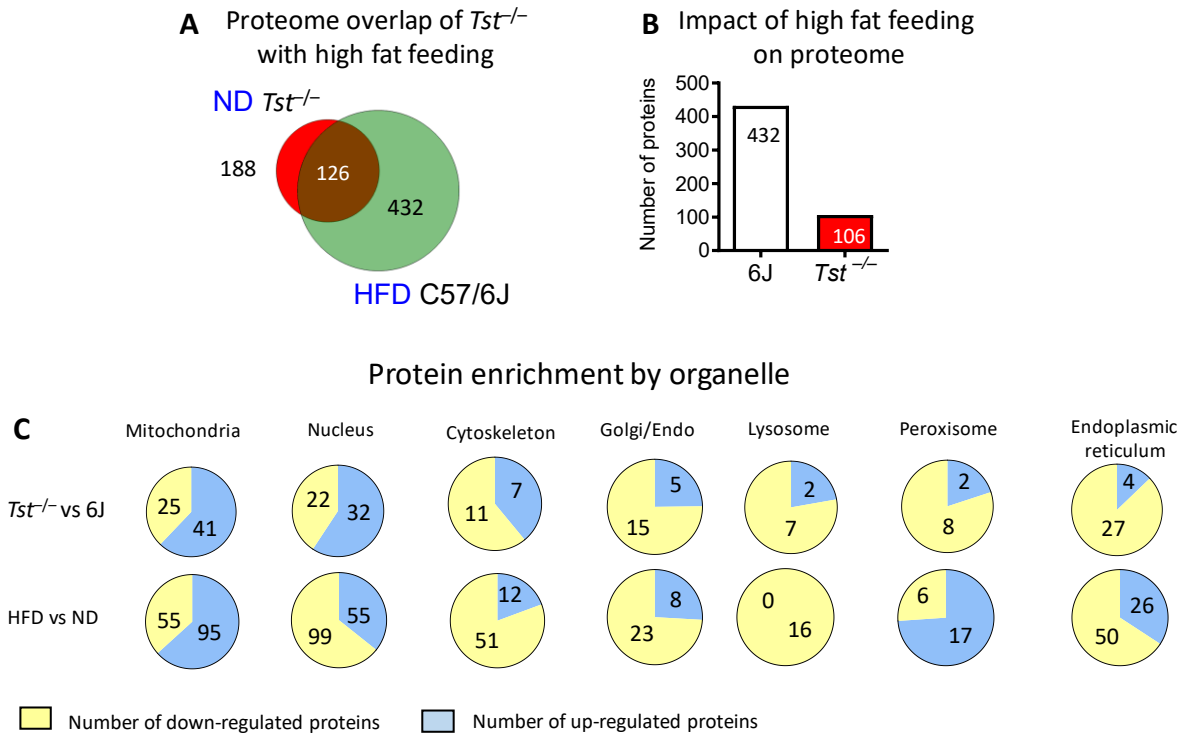

Figure 3. *Tst* deletion engenders a high fat feeding–like hepatic proteome with a distinct organellar signature. (**A**) Venn diagram representing the number of proteins significantly different (at P < 0.01) between normal diet-fed *Tst*$^{-/-}$ and C57Bl/6J (Red circle), and the number of regulated proteins between high fat fed and normal diet-fed C57Bl/6J (Green circle). The overlap (brown) represents those proteins regulated in the same direction by both comparisons (n= 4/genotype). (**B**) Number of proteins significantly different (at p < 0.01) between 58% high fat and normal diet in either C57Bl/6J (white bar), or *Tst*$^{-/-}$ mice (Red bar), (n= 4/genotype). (**C**) Pie charts depicting the proportion of individual liver proteins that are upregulated (Blue space) compared to downregulated (yellow space) after GO term categorisation according to subcellular location. Upper row; normal diet-fed *Tst*$^{-/-}$ relative to normal diet-fed C57Bl/6J. Lower row, high fat-fed C57Bl/6J relative to normal diet-fed C57Bl/6J.

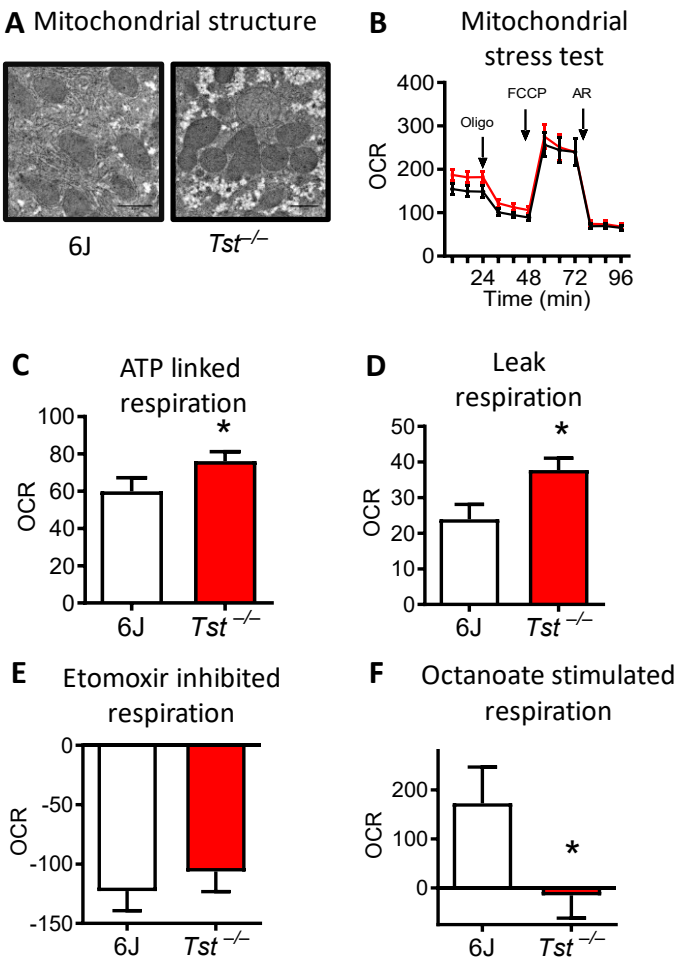

Figure 4. *Tst* deletion results in increased hepatocyte respiration but impaired medium–chain fat respiration. (**A**) Electron microscope images of liver, visualising mitochondria from normal diet-fed C57Bl/6J (n = 4) or *Tst*$^{-/-}$ (n = 4) mice. (**B**) Seahorse trace representing the mean oxygen consumption rate (OCR), normalised to protein, by hepatocytes from normal diet-fed C57Bl/6J (n = 6) or *Tst*$^{-/-}$ (n = 6) mice during a mitochondrial stress test. (**C**) Respiratory OCR linked to ATP production (oligomycin sensitive) by hepatocytes from normal diet-fed C57Bl/6J (n = 6) or *Tst*$^{-/-}$ (n = 6) mice, calculated from Figure 4B. (**D**) Respiratory OCR relating to proton leak (oligomycin insensitive) by hepatocytes from normal diet-fed C57Bl/6J (n = 6) or *Tst*$^{-/-}$ (n = 6) mice, calculated from Figure 4B. (**E**) Reduction of maximal uncoupled respiration following inhibition of long chain fatty acid mitochondrial import using etomoxir (8 µM), from normal diet-fed C57Bl/6J (n = 4) or *Tst*$^{-/-}$ (n = 4) mice. (**F**) Stimulation of maximal uncoupled respiration following addition of medium chain fatty acid octanoate (250 µM), from normal diet-fed C57Bl/6J (n = 4) or *Tst*$^{-/-}$ (n = 4) mice. Data are represented as mean ±SEM. Significance was calculated using an unpaired two tailed, student's t-test (**C**, **D**, **E**, **F**), * $P < 0.05$.

887 # Tables

Table 1. Sulfur species in blood, urine, tissue and cells				
	C57Bl/6J	***Tst*$^{-/-}$**	***Tst*$^{-/-}$/6J ratio**	**Significance**
A Trunk Blood (Micromolar)				
MBB-S (Sulfide)	2.28 +/- 0.43	22.18 +/- 0.85	9.73	****
MBB-SSO3 (Thiosulfate)	n.d.	6.25 +/- 3.17	n.c.	**ns**
B Trunk Plasma (Micromolar)				
MBB-S (Sulfide)	1.88 +/- 0.64	24.50 +/- 2.02	13.03	****
MBB-SSO3 (Thiosulfate)	3.99 +/- 0.99	80.29 +/- 13.6	20.12	**
MBB-GSH (reduced Glutathione)	48.0 +/- 1.15	86.25 +/- 6.27	1.80	***
C Urine (Micromoles/creatine/24hrs)				
MBB-SSO3 (Thiosulfate)	4.99 +/- 2.6	2374 +/- 319	475.75	****
D Inferior Vena Cava (Micromolar)				
MBB-S (Sulfide)	1.22 +/- 0.20	3.58 +/- 0.87	2.93	**ns (0.08)**
MBB-SSO3 (Thiosulfate)	6.58 +/- 4.51	88.3 +/- 13.0	13.42	*
E Liver (µmoles/kg wet liver)				
MBB-S (Sulfide)	13 +/- 1	17 +/- 3	1.31	**ns**
MBB-SSO3 (Thiosulfate)	4 +/- 1	15 +/- 7	3.75	**ns**
DNFB-GSH (reduced Glutathione)	6470 +/- 380	6850 +/- 30	1.04	**ns**
DNFB-Cysteine (Cysteine)	82 +/- 13	67 +/- 11	0.82	**ns**
F Sulfide P3 fluorescence (A510nm/protein)				
Hepatocyte	7.22 +/- 1.00	7.89 +/- 0.80	1.09	**ns**
G Mitochondrial sulfide (MitoA)				
Liver	0.78 +/- 0.16	1.14 +/- 0.45	1.46	**ns**
*** P < 0.05, ** P < 0.01, *** P < 0.001 **** P < 0.0001**				

888

889 **Table 1. *Tst* Deletion Results in Altered Sulfur Metabolites in Blood and Liver.** (**A**) Sulfide dibimane,
890 thiosulfate-MBB, measured by fluorescence detection following HPLC, from whole blood taken from
891 trunk blood of ND-fed C57Bl/6J (n = 4) and *Tst*$^{-/-}$ (n = 4) mice. (**B**) Sulfide dibimane, thiosulfate-MBB,
892 and rGSH-MBB, measured by fluorescence detection following HPLC, from EDTA-Plasma of ND-fed
893 C57Bl/6J (n = 4) and *Tst*$^{-/-}$ (n = 4) mice. (**C**) Thiosulfate-MBB corrected for creatinine from 24 hour
894 urine samples, taken from ND-fed C57Bl6/J (n = 4) and *Tst*$^{-/-}$ (n = 5) mice. (**D**) Sulfide dibimane, and
895 thiosulfate-MBB, from whole blood taken from the inferior vena cava downstream of the hepatic vein
896 of ND-fed C57Bl/6J (n = 3) and *Tst*$^{-/-}$ (n = 3) mice. (**E**) Sulfide dibimane, thiosulfate-MBB, rGSH-MBB,
897 and cysteine-MBB from whole liver (n=4/genotype) of ND-fed C57Bl/6J (n = 4) and *Tst*$^{-/-}$ (n = 4) mice.
898 (**F**) Fluorescence from cultured hepatocytes following incubation with P3 (sulfide reactive probe) from
899 ND-fed C57Bl/6J (n = 4) and *Tst*$^{-/-}$ (n = 4) mice. (**G**) Ratio of Mito N/MitoA from the liver of ND-fed
900 C57Bl/6J (n = 5) and *Tst*$^{-/-}$ (n = 5) mice. Data are represented as mean ±SEM. Significance was
901 calculated using unpaired two-tailed student's t-test. * P < 0.05, ** P < 0.01, *** P < 0.001, **** P <
902 0.0001
903

Table 2. GO Terms Persulfidation rate (*Tst*$^{-/-}$ vs C57Bl/6J liver, ND-fed)			
GO-ID	**Name**	**Direction (*Tst*$^{-/-}$ vs 6J)**	**Genes**
	GO terms Identified by log fold change		
0050660	FAD binding	Decreased	12
0008168	Methyltransferase activity	Decreased	9
0016741	Transferase activity, transferring one-carbon groups	Decreased	9
0008565	Protein transporter activity	Decreased	8
0008238	Exopeptidase activity	Decreased	7
0005777	Peroxisome	Decreased	7
0042579	Microbody	Decreased	7
0003995	Acyl-CoA dehydrogenase activity	Decreased	6
0008483	Transaminase activity	Decreased	6
0016769	Transferase activity, transferring nitrogenous groups	Decreased	6
0008757	S-adenosylmethionine-dependent methyltransferase activity	Decreased	6
0016655	Oxidoreductase activity, acting on NADH/NADPH, quinone	Decreased	5
0004177	Aminopeptidase activity	Decreased	5
0000059	Protein import into nucleus, docking	Decreased	3
0005643	Nuclear pore	Decreased	3
0031965	Nuclear membrane	Decreased	3
0044453	Nuclear membrane part	Decreased	3
0046930	Pore complex	Decreased	3
0015629	Actin cytoskeleton	Decreased	3
0016652	Oxidoreductase activity, NADH/NADPH, NAD/NADP acceptor	Decreased	3
0050662	Coenzyme binding	Increased	5
0016651	Oxidoreductase activity, NADH/NADPH,	Increased	5
0003954	NADH dehydrogenase activity	Increased	4
0008137	NADH dehydrogenase (ubiquinone) activity	Increased	4
0050136	NADH dehydrogenase (quinone) activity	Increased	4
0006739	NADP metabolism	Increased	3
0006769	Nicotinamide metabolism	Increased	3
0006733	Oxidoreduction coenzyme metabolism	Increased	3

904

905 **Table 2. Tst Deletion Results in Differential Persulfidation Rate of Liver Proteins**. Significant GO terms
906 represented by peptides with different persulfidation rates in the ND-fed *Tst*$^{-/-}$ liver relative to
907 C57Bl/6J. '**Direction**' indicates whether the persulfidation is decreased or increased in *Tst*$^{-/-}$ relative
908 to C57Bl/6J. '**Genes**' indicates the number of genes in the *Tst*$^{-/-}$ that represent the changes driving
909 the GO term.
910

911

912

913

914

Table 3. KEGG pathways (*Tst*$^{-/-}$ vs C57Bl/6J liver, ND-fed)			
Entry	**Name**	**Genes**	**Significance**
A. Increased in ND *Tst*$^{-/-}$ liver			
00250	Alanine, Aspartate and glutamate metabolism	6	***
00260	Glycine, serine and threonine metabolism	5	**
00270	Cysteine and methionine metabolism	4	*
04122	Sulfur relay system	2	*
B. Reduced in ND *Tst*$^{-/-}$ liver			
00980	Metabolism of xenobiotics by cytochrome P450	12	****
00982	Drug metabolism – cytochrome P450	12	****
05204	Chemical carcinogenesis	12	****
00480	Glutathione metabolism	8	***
00040	Pentose and glucoronate interconversions	5	**
04142	Lysosome	6	**
04390	Hippo signalling pathway	4	**
00500	Starch and sucrose metabolism	5	**
05215	Prostate cancer	3	**
04024	cAMP signalling pathway	4	*
04141	Protein processing in ER	9	*
05211	Renal cell carcinoma	3	*
00830	Retinol metabolism	6	*
00053	Ascorbate and aldarate metabolism	4	*
00860	Porphyrin and chlorophyll metabolism	4	*
04722	Neurotrophin signalling pathway	3	*
04670	Leukocyte transendothelial migration	4	*
04010	MAPK signalling pathway	4	*
04720	Long-term potentiation	2	*
04914	Progesterone-mediated oocyte maturation	2	*
04062	Chemokine signalling pathway	3	*
04110	Cell cycle	3	*
04015	Rap1 signaling pathway	4	*
00983	Drug metabolism - other enzymes	5	*
04918	Thyroid hormone synthesis	3	*
04612	Antigen processing and presentation	3	*
05203	Viral Carcinogenesis	5	*
*** P < 0.05, ** P < 0.01, *** P < 0.001 **** P < 0.0001**			

915

916 **Table 3. Tst Deletion Results in Differential Hepatic Protein Abundance of KEGG Pathways.** (**A**)
917 Significant KEGG pathway terms represented by proteins that are more abundant in the ND-fed *Tst*$^{-}$
918 $^{/-}$ liver compared with ND-fed C57Bl/6J. (**B**) Significant KEGG pathway terms represented by proteins
919 that are less abundant in the ND-fed *Tst*$^{-/-}$ liver compared with ND-fed C57Bl/6J. '**Genes**' indicates
920 the number of genes in the *Tst*$^{-/-}$ that represent the changes driving the KEGG pathway.

921

922

923

Table 4. GO Terms Congruence of Abundance and Persulfidation

GO-ID	Name	Persulfidation ($Tst^{-/-}$ vs 6J)	Abundance ($Tst^{-/-}$ vs 6J)
0008483	Transaminase activity	Decreased	Increased
0016769	Transferase activity, transferring nitrogenous	Decreased	Increased
0003995	Acyl-CoA dehydrogenase activity	Decreased	Decreased
0005777	Peroxisome	Decreased	Decreased
0042579	Microbody	Decreased	Decreased

924

925 **Table 4. The *Tst*$^{-/-}$ liver proteome and persulfidome converges on lipid oxidation pathways.** GO
926 terms that are significantly regulated following comparison of ND-fed *Tst*$^{-/-}$ relative to C57Bl/6J, at *both* the
927 level of cysteine persulfidation and protein abundance.

928

929